



Probabilistic risk assessment of gold nanoparticles after intravenous administration by integrating in vitro and in vivo toxicity with physiologically based pharmacokinetic modeling

Yi-Hsien Cheng, Jim E. Riviere, Nancy A. Monteiro-Riviere & Zhoumeng Lin

To cite this article: Yi-Hsien Cheng, Jim E. Riviere, Nancy A. Monteiro-Riviere & Zhoumeng Lin (2018) Probabilistic risk assessment of gold nanoparticles after intravenous administration by integrating in vitro and in vivo toxicity with physiologically based pharmacokinetic modeling, *Nanotoxicology*, 12:5, 453-469, DOI: [10.1080/17435390.2018.1459922](https://doi.org/10.1080/17435390.2018.1459922)

To link to this article: <https://doi.org/10.1080/17435390.2018.1459922>



View supplementary material [↗](#)



Published online: 14 Apr 2018.



Submit your article to this journal [↗](#)



Article views: 78



View related articles [↗](#)



View Crossmark data [↗](#)



Citing articles: 1 View citing articles [↗](#)

ARTICLE



Probabilistic risk assessment of gold nanoparticles after intravenous administration by integrating *in vitro* and *in vivo* toxicity with physiologically based pharmacokinetic modeling

Yi-Hsien Cheng^a , Jim E. Riviere^a , Nancy A. Monteiro-Riviere^b  and Zhoumeng Lin^a 

^aInstitute of Computational Comparative Medicine (ICCM), Department of Anatomy and Physiology, College of Veterinary Medicine, Kansas State University, Manhattan, KS, USA; ^bNanotechnology Innovation Center of Kansas State (NICKS), Department of Anatomy and Physiology, College of Veterinary Medicine, Kansas State University, Manhattan, KS, USA

ABSTRACT

This study aimed to conduct an integrated and probabilistic risk assessment of gold nanoparticles (AuNPs) based on recently published *in vitro* and *in vivo* toxicity studies coupled to a physiologically based pharmacokinetic (PBPK) model. Dose–response relationships were characterized based on cell viability assays in various human cell types. A previously well-validated human PBPK model for AuNPs was applied to quantify internal concentrations in liver, kidney, skin, and venous plasma. By applying a Bayesian-based probabilistic risk assessment approach incorporating Monte Carlo simulation, probable human cell death fractions were characterized. Additionally, we implemented *in vitro* to *in vivo* and animal-to-human extrapolation approaches to independently estimate external exposure levels of AuNPs that cause minimal toxicity. Our results suggest that under the highest dosing level employed in existing animal studies (worst-case scenario), AuNPs coated with branched polyethylenimine (BPEI) would likely induce ~90–100% cellular death, implying high cytotoxicity compared to <10% cell death induced by low-to-medium animal dosing levels, which are commonly used in animal studies. The estimated human equivalent doses associated with 5% cell death in liver and kidney were around 1 and 3 mg/kg, respectively. Based on points of departure reported in animal studies, the human equivalent dose estimates associated with gene expression changes and tissue cell apoptosis in liver were 0.005 and 0.5 mg/kg, respectively. Our analyses provide insights into safety evaluation, risk prediction, and point of departure estimation of AuNP exposure for humans and illustrate an approach that could be applied to other NPs when sufficient data are available.

ARTICLE HISTORY

Received 8 August 2017
Revised 23 March 2018
Accepted 26 March 2018

KEYWORDS



Gold nanoparticle;
computational nanotoxicology;
physiologically based
pharmacokinetic modeling;
probabilistic risk assessment


Introduction

Recent advancements in nanotechnology have identified promising engineered nanomaterials (or nanoparticles, NPs) for various applications, including disease diagnostics and therapeutics. Amongst the myriad of NPs available, gold nanoparticles (AuNPs) have great potential for wide applications in nanomedicine due to their unique physical, chemical, and optoelectronic properties. Specifically, AuNPs can serve as either diagnostic or therapeutic agents for tumors or rheumatoid arthritis, or as carriers for delivery of drugs, antigens, peptides, and genetic materials (Arvizo et al. 2012; Jain et al. 2012). The use of AuNPs inevitably increases the likelihood of unintentional low-dose environmental exposure,

occupational exposure, and intentional high-dose exposure for medical purposes; raising concern about the potential short-term and long-term adverse effects on human health (Khlebtsov and Dykman 2011). Despite these exposures, the potential risk of AuNPs has not been well characterized.

Numerous *in vivo* and *in vitro* studies have investigated the potential toxicity of AuNPs. Zhang et al. (2011) reported that exposure to 10 and 60 nm polyethylene glycol (PEG)-coated AuNPs after intraperitoneal injection caused significant increase in alanine transaminase and aspartate transaminase and decrease in creatinine, suggesting liver and kidney damage in mice, while 5 and 30 nm AuNPs caused relatively lower toxicity, implying

CONTACT Zhoumeng Lin  zhoumeng@ksu.edu  Institute of Computational Comparative Medicine (ICCM), Department of Anatomy and Physiology, College of Veterinary Medicine, Kansas State University, 1800 Denison Avenue, P200 Mosier Hall, Manhattan, KS 66506, USA

 Supplemental data for this article can be accessed [here](#).

© 2018 Informa UK Limited, trading as Taylor & Francis Group

size-dependent toxicity. Cho et al. (2009) demonstrated dose-dependent liver toxicity in mice exposed to 13 nm PEG-coated AuNPs after intravenous injection. *In vitro* studies based on human- or animal-derived cells have also suggested dose-dependent cytotoxicity of AuNPs (Pernodet et al. 2006; Mannerström et al. 2016). Additionally, a bio-corona which forms instantly upon contact with biological fluids as biomolecules attaching to the NP surface has also been shown to modulate AuNPs cellular uptake and toxicity (Westmeier et al. 2016; Chandran et al. 2017). One challenge in this field is that the existing AuNP toxicity studies have used different study designs (cell types, media composition, particle characterization methods, and biomarkers of cytotoxicity) with different types of AuNPs (i.e. varied in size, shape, dose, and surface functionalization) that prevent integrating available experimental evidence into a comprehensive systematic evaluation.

To conduct such an integrated risk assessment of AuNPs, we determined the dose-dependent cytotoxicity of different sizes (40 and 80 nm) of AuNPs coated with PEG, branched polyethylenimine (BPEI), or lipoic acid (LA) that were pre-incubated with human plasma proteins (HP) or human serum albumin (HSA) (to form defined protein coronas), or without pre-incubation with proteins (bare) in four human cell types, including hepatocytes (Choi et al. 2017), umbilical vein endothelial cells (HUVEC) (Chandran et al. 2017), renal proximal tubule epithelial cells (HRPTEC) (Ortega et al. 2017), and keratinocytes (Li and Monteiro-Riviere 2016). Additionally, we used our recently developed physiologically based pharmacokinetic (PBPK) model for AuNPs in mice and rats that had been successfully extrapolated to humans (Lin et al. 2016a, 2016b; Lin et al. 2017). This model allows one to conduct *in vitro* to *in vivo* extrapolation (IVIVE) and cross-species extrapolation of the dosimetry and toxicity of AuNPs, thereby providing a basis for quantitative risk assessment.

The objective of this study was to conduct an integrated and probabilistic risk assessment of AuNPs in humans after intravenous (IV) administration, which is the most commonly used administration route in animal studies and in humans for biomedical application. Specifically, this study aimed to (i) conduct dose-response relationship analyzes

based on our reported *in vitro* toxicity studies, (ii) implement the validated human PBPK model incorporating Monte Carlo simulation to estimate internal dosimetry under various exposure scenarios, (iii) characterize the potential risk of AuNPs under different exposure scenarios using a Bayesian-based probabilistic risk assessment framework (NRC 2009; EPA 2014; Cheng et al. 2016), and (iv) explore several points of departure (PODs) for AuNP exposure by reconstructing exposure dosimetry based on either *in vitro* or *in vivo* biological responses.

Materials and methods

Modeling framework

To assess the potential risks of AuNPs to humans, we applied a probabilistic approach based on US EPA guidelines (NRC 2009; EPA 2014). Figure 1 represents a conceptual framework depicting the general process in probabilistic risk assessment that contains four critical elements; hazard identification, dose-response analysis, exposure analysis, and risk characterization. In addition, this study estimated the human equivalent dose (HED) associated with reported or estimated PODs (NOAEL and LOAEL [no and lowest observed adverse effect levels, respectively] and EC_5 and EC_{10} [exposure concentrations causing 5% and 10% maximum cell death, respectively]) based on *in vivo* or *in vitro* toxicity studies using the human PBPK model. We term this process exposure reconstruction (detailed below).

Hazard identification

To determine the potential toxicity of AuNPs, we conducted a comprehensive evaluation of the effects of various types of AuNPs on the viability of different human cell types, including hepatocytes (Choi et al. 2017), HUVEC (Chandran et al. 2017), HRPTEC (Ortega et al. 2017), and keratinocytes (Li and Monteiro-Riviere 2016) using the same AuNPs. The experimental designs of these studies were similar. In brief, cells were exposed for 24 h to different concentrations (e.g. 0–400 $\mu\text{g/mL}$ for hepatocytes) of spherical Biopure™ 40 or 80 nm AuNPs coated with PEG (neutral), BPEI (positive), or LA (negative) (nanoComposix, San Diego, CA) that were pre-incubated with HP or HSA, or without pre-incubation with proteins (bare). Cell viability was

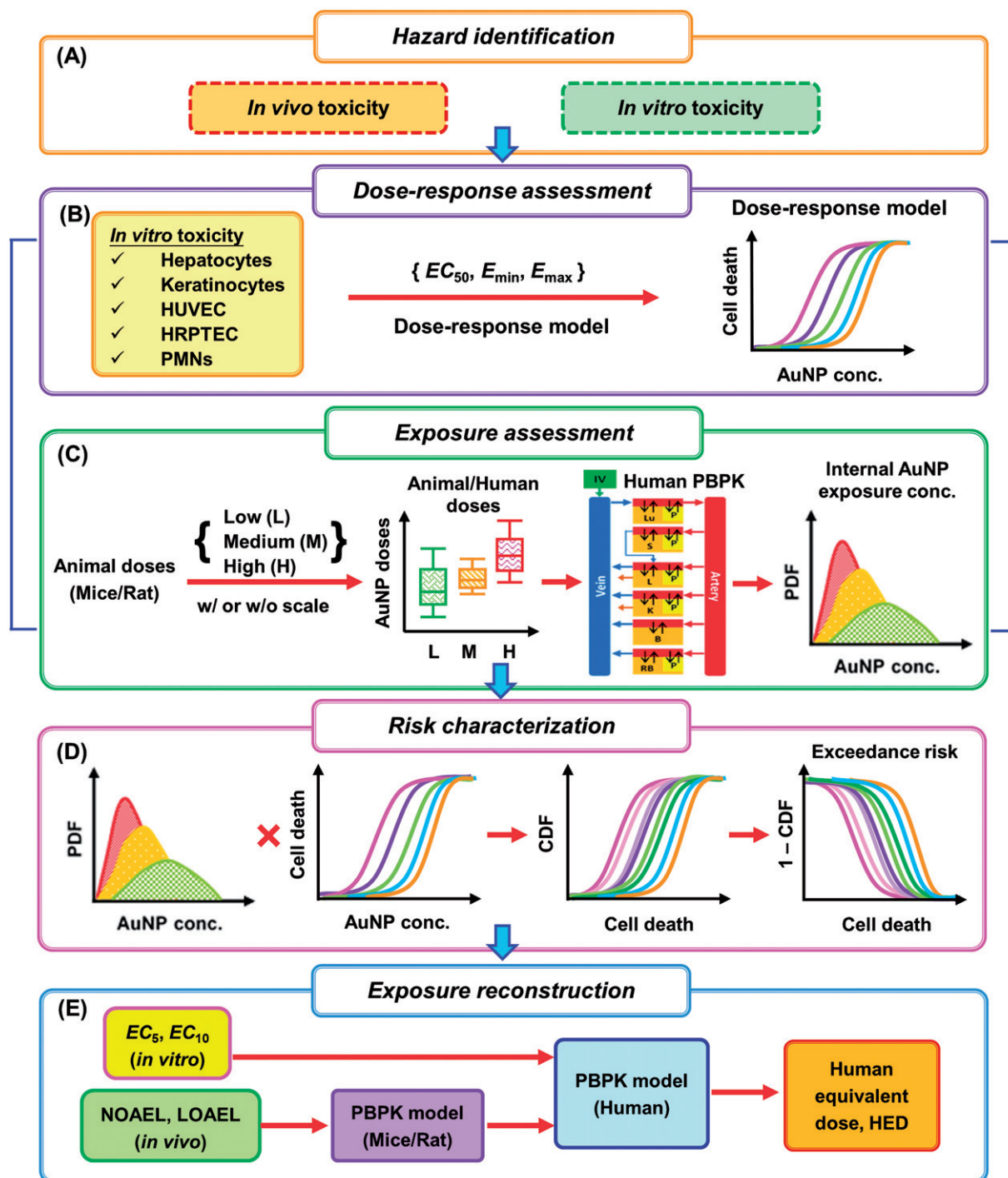


Figure 1. A flowchart of the probabilistic risk assessment approach. *Abbreviations:* HUVEC: human umbilical vein endothelial cells; HRPTEC: human renal proximal tubule epithelial cells; PMNs: human polymorphonuclear neutrophil cells; E_{min} and E_{max} : minimum and maximum fractional cell death; EC_5 , EC_{10} , and EC_{50} : exposure concentration causing 5%, 10%, and 50% maximum cell death, respectively; n : Hill coefficient; PDF: probability density function; CDF: cumulative distribution function; NOAEL and LOAEL: no and lowest observed adverse effect level, respectively.

determined using the alamarBlue assay as previously described (Monteiro-Riviere et al. 2009). Note that only the 40 and 80 nm AuNPs coated with BPEI and BPEI-HP were found to cause significant cytotoxicity in selected cell types.

Besides toxicity data from our own group, we also included data from an independent study in which the apoptotic effect of AuNPs on human neutrophils (polymorphonuclear neutrophil cells, PMNs) was determined (Noël et al. 2016). Briefly, PMNs

were exposed to different concentrations of PELCO® BioPure™ 20 or 70 nm AuNPs (Ted Pella, Redding, CA) for 24 h and apoptosis was assessed by counting Hema 3-stained PMN with light microscopy. Additional information on the experimental designs and physicochemical properties of studied AuNPs is provided in the studies listed in [Supplementary Table S1](#). The cytotoxicity data from selected studies were used for subsequent dose–response analyses.

Dose–response assessment

To investigate dose dependency of AuNP-induced cytotoxicity, several commonly applied quantal models, including exponential, Weibull, Logistic, and Hill models were adopted to reconstruct dose–response relationships (WHO 2009; EPA 2012) (Figure 1(B)).

$$\text{Exponential: } P(E|C) = E_{\max} - \exp(-\beta \times C) + E_{\min}, \quad (1)$$

$$\text{Weibull: } P(E|C) = E_{\max} (\exp(-(E_{\min} + (\beta \times C)^\gamma))), \quad (2)$$

$$\text{Logistic: } P(E|C) = \frac{E_{\max} - E_{\min}}{1 + \exp(\alpha - \beta \times C)} + E_{\min}, \quad (3)$$

$$\text{Hill: } P(E|C) = \frac{(E_{\max} - E_{\min}) \times C^n}{(EC_{50}^n + C^n)} + E_{\min}, \quad (4)$$

where $P(E|C)$ is the conditional probability representing the probability that a certain effect (i.e. a certain fraction of cell death) may occur at a given AuNP exposure concentration, E_{\min} and E_{\max} represent minimum and maximum fractional cell death, respectively, EC_{50} is the exposed concentration leading to half maximum cell death fraction ($\mu\text{g/ml}$), α is the parameter indicating location in the Logistic model, γ is the exponent parameter in the Weibull model, and β (as in exponential, Logistic, and Weibull models) and n (referred to as the Hill coefficient in Hill model) are slope factors that determine the overall shape of the dose–response curve. A commercial software package TableCurve 2D™ (Version 5.1.2, Systat Software Inc., San Jose, CA) was employed to perform nonlinear curve fitting to derive the optimal fitting model based on the goodness-of-fit (determination of coefficient, r^2) and to determine the parameter values using the least-square method with a p value of <0.05 considered as statistically significant.

In this study, we employed the administered/applied *in vitro* concentrations in the dose–response analyses of the selected *in vitro* toxicity data. Multiple studies have shown that the delivered

dose is a more appropriate dose metric than the administered dose/concentration in the interpretation of *in vitro* toxicity data for NPs (Hinderliter et al. 2010; Cohen et al. 2014; DeLoid et al. 2017). In this regard, we also applied a commonly used model (i.e. the *in vitro* sedimentation, diffusion, and dosimetry [ISDD] model) to predict the deposited fractions of AuNPs after different times of exposure based on the experimental condition in Choi et al. (2017). The results showed that at 24 h post-exposure to bare AuNPs, up to 100% (i.e. 83–100%) of the applied dose would be deposited to the bottom of the cell culture plate ([Supplementary Table S2](#)). Ideally, it would be optimal to use the ISDD model-predicted delivered dose to conduct the dose–response analysis. However, the ISDD model-predicted delivered dose is typically in the unit of pg NPs per cell (pg/cell) or number of NPs per cell. At this stage, it cannot be smoothly integrated with our PBPK model simulation result, which is typically in a unit of μg per g tissue ($\mu\text{g/g}$), representing the overall concentration of NPs in the organ. In order to fully integrate ISDD model with PBPK model, we will need a more detailed mechanistic model that simulates the distribution of NPs at both the cellular and organ level, so that we can use the PBPK model to simulate the concentration of NPs in individual cells. This is a future research direction once additional data become available.

Exposure analysis

To quantify internal exposure concentrations of AuNPs in human target tissues or organs after IV administration, the previously validated human PBPK model extrapolated from rats was implemented (Lin et al. 2016a). In brief, the human PBPK model contained seven compartments; including plasma, lungs, liver, kidneys, spleen, brain, and rest of body ([Supplementary Figure S1](#)). To better describe the biodistribution of AuNPs, a membrane-limited model structure incorporating endocytosis of AuNPs from plasma to tissue phagocytic cells (PCs) was adopted (Lin et al. 2016a, 2016b). Except for plasma and brain, all compartments were divided into three sub-compartments as capillary blood, tissue, and PCs. All the physiological and AuNP-specific parameters used in the validated

human PBPK model were kept the same as in the original model and provided in our previous work (referred to [Supplementary Tables 2 and 3](#) in Supporting Information from Lin et al. 2016a). The complete human PBPK model code is provided in the [Supplementary Material](#).

A wide range of IV administered doses (0.001–100 mg/kg) that have been applied in animal studies (mice or rats) (Khlebtsov and Dykman 2011; Lin et al. 2015) was selected to derive the associated human doses in order to predict internal tissue exposure concentrations in humans. To better determine the levels of AuNPs in human tissues and to assess the potential risks after IV administration with different dose levels, we categorized the animal IV dosages into three dosing windows as low (<0.1 mg/kg), medium (0.1–10 mg/kg), and high (>10 mg/kg), respectively based on the frequency of a specific dosing window as reported in Khlebtsov and Dykman (2011). This categorization only applies to IV administration in the present study and it is consistent with the dose stratification in our earlier study (Lin et al. 2016a). Among the reported animal IV doses included in Khlebtsov and Dykman (2011), the low-to-medium IV dose range was commonly used and only a few studies used the high IV dose window. Since we utilized a species-specific and physiologically based modeling approach, we directly incorporated the animal doses into the human PBPK model to assess the potential risks in humans exposed to doses used in animal studies. Additionally, in clinical pharmacology, it is a common practice to use an allometric approach in the translation of doses between two different species and estimation of a more accurate starting dose for clinical trials, provided considering species differences in pharmacokinetic parameters such as clearance and volume of distribution (Sharma and McNeill 2009). Therefore, we also assessed the potential risks in humans exposed to human doses (HD) that were scaled from animal doses (AD) based on reported conversion factors (K_m) using the following equation (Sharma and McNeill 2009; Nair and Jacob 2016),

$$\text{HD (mg/kg)} = \text{AD (mg/kg)} \times \left(\frac{K_{m,m} \text{ or } K_{m,r}}{K_{m,h}} \right), \quad (5)$$

where $K_{m,m}$, $K_{m,r}$, and $K_{m,h}$ represent conversion factors associated with the body surface area and

body weight in mice (20 g, $K_{m,m}=3$), rats (250 g, $K_{m,r}=7$), and humans (70 kg, $K_{m,h}=37.8$), respectively (Nair and Jacob 2016).

In this study, we applied two different approaches to derive the human doses for assessing the potential risks in order to compare the differential risks between our PBPK approach and the PBPK+allometric approach. The allometric approach is commonly used for small molecular drugs, but its application for NPs has not been validated. Additional studies are needed to test whether the allometric approach is applicable or necessary to NPs. [Supplementary Table S3](#) summarizes IV administered dosages of AuNPs applied in animal studies and the associated scaled dosages that were implemented in human PBPK modeling. Results of both approaches were compared and discussed below.

The random-sampling Monte Carlo simulation technique was implemented while scaling low, medium, and high AD (LAD, MAD, and HAD) to the associated low, medium, and high HD (LHD, MHD, and HHD) in order to consider variability and uncertainty within each dosing range (Bois et al. 2010; Cheng et al. 2016; Shi et al. 2016). Monte Carlo simulation was performed with 10,000 iterations via the software Crystal Ball® (Version 11.1.2.4, Oracle Corporation, Redwood Shores, CA) as an add-in within Microsoft Excel (Version 2016) to ensure the stability of input dose distribution profiles. Specifically, the minimum and maximum values of a specific AD or HD range were assigned as 1st and 99th percentile of a lognormal (LN) distribution (i.e. to define the assumption in Crystal Ball) to generate the mean dose and the standard deviation (SD) of a particular dose window (i.e. to generate the forecast in Crystal Ball). The LN distribution was found to be the optimal distribution based on the K-S value of the Kolmogorov–Smirnov test. This same procedure was applied to estimate the mean and SD values for the LAD, MAD, HAD ranges (non-scaled), as well as the LHD, MHD, and HHD ranges (allometry-scaled) (Figure 1(C) and [Supplementary Table S3](#)).

Since our PBPK model only contains plasma, lungs, liver, kidneys, spleen, brain, and rest of body compartments, we could not directly estimate internal concentrations of AuNPs in endothelial cells and keratinocytes using the model. We alternatively estimated internal concentrations in venous plasma

and rest of body as surrogates for internal concentration in endothelial cells and keratinocytes, respectively. This was done because endothelial cells are in direct contact with the plasma and the skin is a major part of the rest of body compartment in our model. We acknowledged that this will introduce some uncertainty to our analysis. A more detailed mechanistic PBPK model would help improve our analysis, but it would require additional data for model construction, which is a future research direction.

Maximum internal exposure concentrations (C_{\max}) in venous plasma, liver, kidney, and rest of body were then estimated by incorporating the LN distributed ADs and HDs into the human PBPK model using Berkeley MadonnaTM (Version 8.3.23, University of California at Berkeley, CA). There is no a built-in function in Berkeley Madonna to perform Monte Carlo simulation for LN distribution. Since the lognormal distribution is a continuous probability distribution of a random variable whose logarithm is normally distributed, we applied the inverse natural logarithmic transformation of the "NORMAL" function to produce lognormally distributed random numbers based on our recently published method (Li et al. 2017a). After incorporating the LN distributed doses into the human PBPK model, 1000 simulations were performed in Berkeley Madonna to compute internal concentrations in liver, kidney, venous plasma, and rest of body (mean \pm SD) underlying different exposure scenarios. Here we simulated only 24-h biodistribution data according to the exposure durations in selected *in vitro* studies. Finally, we performed 10 000 Monte Carlo simulations using Crystal Ball to select the optimal distribution based on Kolmogorov–Smirnov statistics and to estimate associated probability density functions (PDFs) for maximum internal exposure concentrations (i.e. the frequency or probability of a specific internal concentration to occur).

Risk characterization

To further characterize the human exposure risk after IV administration of AuNPs, this study implemented a Bayesian-based probabilistic risk assessment model by linking the AuNP-PBPK exposure model with the dose–response model. Specifically, the optimized distribution profiles as well as PDFs

of maximum internal AuNP exposure concentrations in humans under various dosing ranges, $P(C)$ (i.e. the prior probability), were estimated based on the simulated results obtained from the human AuNP-PBPK model (Figure 1(C)). A likelihood $P(E|C)$ (i.e. the likelihood that a certain endpoint (e.g. fractional cell death) may occur at a given exposure concentration of AuNPs) was obtained from the best-fitted dose–response profiles (Figure 1(B)). This study then added up the PDF of the prior probability to estimate the cumulative distribution function (CDF) for following analyzes using the Bayesian inference.

Followed by the Bayesian inference, a CDF describing cumulative risk probability of a specific extent of human cell death endpoint to occur at a particular AuNP exposure concentration corresponded to a specific cumulative probability, was derived by combining both prior probability (Figure 1(C)) and likelihood (Figure 1(B)), resulting in a posterior probability, $P(C|E)$ (Figure 1(D)), estimate:

$$P(C|E) = P(C) \times P(E|C). \quad (6)$$

This analysis then converted cytotoxicity–cumulative risk probability profile into exceedance risk profile. The exceedance risk profile represents the probable exceedance probability for a specific cell death fraction to occur at a particular exposure dose/concentration and can be calculated as "1 – CDF", e.g. an exceedance probability of 0.5 suggests there is 50% chance (i.e. likely) for cellular death to exceed a particular fraction at a given exposure.

Exposure reconstruction using *in vitro* to *in vivo* extrapolation approach

Two PODs estimated from *in vitro* dose–response relationships using the Hill model (EC_5 and EC_{10}) were considered for estimating the associated administered external dosing levels in humans (i.e. HED). Specifically, this study first estimated mean and 95% confidence interval (CI) values of EC_5 and EC_{10} for different human cell types via TableCurve 2D. Berkeley Madonna was then applied to estimate the exact administration dosages that would result in maximum target organ concentrations that were equal to mean and 95% CIs of EC_5 and EC_{10} using the human PBPK model. We termed the process of estimating administered HEDs through the human PBPK model based on PODs derived from the

in vitro dose–response models as reverse dosimetry analysis or exposure reconstruction.

Exposure reconstruction using animal-to-human extrapolation approach

This study also estimated the HEDs associated with reported PODs (e.g. NOAEL or LOAEL) based on endpoints previously calculated from animal studies (Cho et al. 2009; Balasubramanian et al. 2010). Explicitly, Balasubramanian et al. (2010) performed an *in vivo* study to investigate biodistribution and toxicity after single IV injection of 0.01 mg/kg AuNPs in rats for up to 2 months, and observed significant changes on the expression of genes related to detoxification, lipid metabolism, and cell cycle effects in target organs liver and spleen. Among the published toxicity studies of AuNPs investigating the adverse outcomes in rodents, this is the study that reported significant toxicity at the lowest administered dose. Therefore, we considered this dose as LOAEL for the endpoint of gene expression changes. Additionally, Cho et al. (2009) conducted a biodistribution study with IV administered dosages ranging from 0.17 to 4.26 mg/kg and used a TUNEL (terminal deoxynucleotidyl transferase-mediated dUTP nick end-labeling) assay to detect apoptosis in mouse liver tissue. The NOAEL and LOAEL were reported to be 0.85 and 4.26 mg/kg, respectively. The reported NOAEL and/or LOAEL were then incorporated into our published mouse or rat PBPK model (Lin et al. 2016a) to estimate the corresponding maximum liver concentration. Assuming that the same effect in humans would occur if the target organ liver concentration in rodents is the same as in humans, HEDs associated with reported PODs in rodents can then be determined based on the human PBPK model through a reverse dosimetry analysis (WHO 2010).

Results

In vitro dose–response relationships

Our earlier study (Choi et al. 2017) showed that only AuNPs coated with BPEI with or without HP protein coronas caused significant cytotoxicity in human hepatocytes. To determine the optimal dose–response model for describing AuNP exposure concentration corresponded cellular death in hepatocytes, the differences in goodness-of-fit (r^2 values)

and parameter estimates of constructed models were compared and summarized in [Supplementary Table S4](#). Among the constructed dose–response relationships, the Hill model has superior goodness-of-fit for hepatocyte toxicity data compared to other models, including exponential, Weibull, and Logistic models ([Supplementary Table S4](#) and Figure S2). In addition, the Hill model can describe cytotoxic response at both low and high exposure concentrations more adequately than other models. Therefore, we selected Hill model to describe an individual *in vitro* dose–response relationships afterwards. [Figure 2\(A–D\)](#) demonstrated that the Hill model adequately characterized the relationship between the exposure concentration of AuNPs and the corresponding observed cytotoxicity in hepatocytes ($r^2 = 0.90–0.99$, $p < 0.001$) ([Table 1](#)). Among the studied AuNPs of different sizes and surface coatings, 40 nm bare AuNP-BPEI is the most toxic with EC_{50} estimated to be 185 $\mu\text{g/ml}$ (95% CI: 167–203 $\mu\text{g/ml}$) and >90% cell death under maximum exposure concentration of 400 $\mu\text{g/ml}$ ([Figure 2\(A\)](#)). In contrast, AuNP-BPEI coated with HP coronas had substantially lower cytotoxicity with EC_{50} (mean \pm SE) estimated to be 273 ± 23 and 395 ± 5 $\mu\text{g/ml}$ for 40 and 80 nm AuNP-BPEI-HP, respectively ([Figure 2\(C,D\)](#), [Table 1](#)).

For other human cells, 40 and 80 nm bare AuNP-BPEI-induced cytotoxicity can be well characterized with the Hill model as well ($r^2 = 0.91–0.98$, $p < 0.001$) ([Figure 3\(A–E\)](#), [Table 1](#)). Based on the fitted results, AuNP-BPEI-induced cell death fractions were similar among human keratinocytes, HUVEC, and HRPTEC cells with EC_{50} estimates ranging from 62 to 81 $\mu\text{g/ml}$ and with 70–81% cell death under 100 $\mu\text{g/ml}$ bare AuNP-BPEI exposure ([Figure 3\(A–E\)](#), [Table 1](#)). Additionally, 40 nm bare AuNP-PEG caused relatively low, but quantifiable cytotoxicity to HUVEC compared to bare 40 nm AuNP-BPEI with cell death fraction estimated around 21% under 200 $\mu\text{g/ml}$ bare AuNP-PEG exposure ([Figure 3\(F\)](#), [Table 1](#)). For PMNs, instead of fixing E_{max} to 1, optimally fitted E_{max} estimates of 0.60 and 0.83 were adopted because observed toxicity data close to 100% cell death were not available. The Hill model provided statistically significant and acceptable fitting results with Hill coefficients n estimated to be 0.29 ($r^2 = 0.63$, $p < 0.001$) and 0.47 ($r^2 = 0.81$, $p < 0.001$), respectively. However, the dose-dependence in

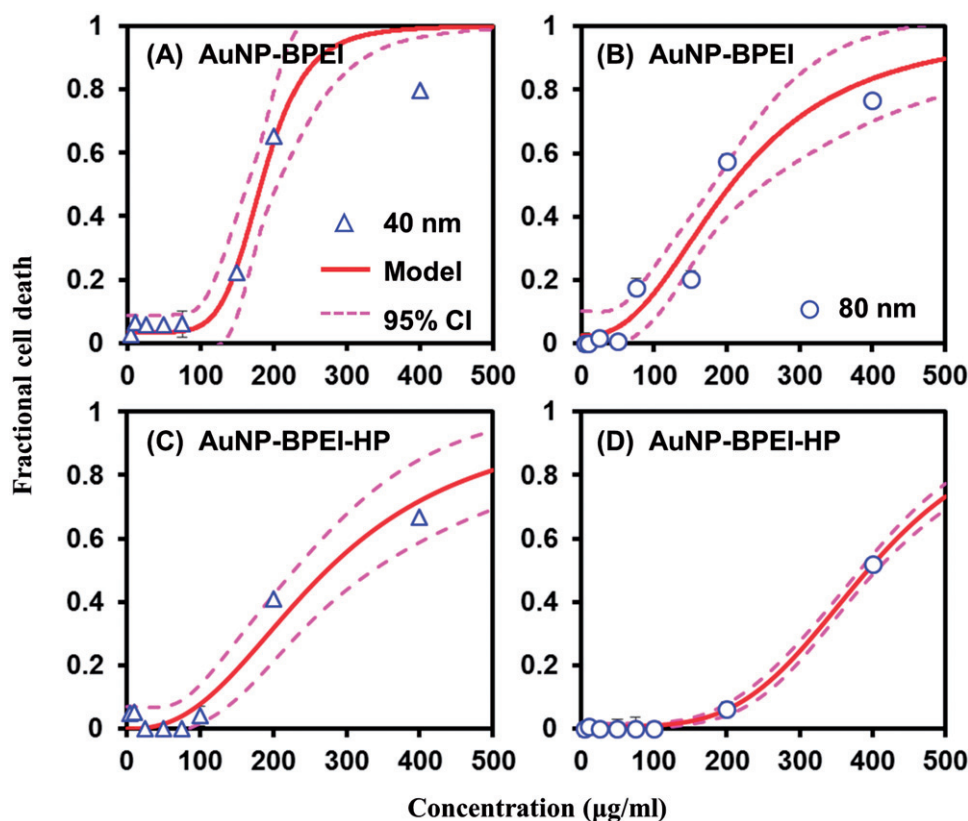


Figure 2. Fitted response curves for concentration-dependent cell death fraction in hepatocytes exposed to (A) 40 nm bare AuNP-BPEI, (B) 80 nm bare AuNP-BPEI, (C) 40 nm AuNP-BPEI-HP, and (D) 80 nm AuNP-BPEI-HP, respectively. AuNP: gold nanoparticle; BPEI: branched polyethylenimine; HP: human plasma proteins.

AuNP-induced PMN toxicity was not obvious ($n < 1$) (Figure 3(G,H), Table 1).

External and internal exposure concentration estimates

Figure 4(A–C) displays human IV dosages associated directly with animal dosing levels (LAD, MAD, and HAD) (i.e. without scaling). Based on Monte Carlo simulation results, the median dose estimates for LAD, MAD, and HAD were ~ 0.06 , 0.8, and 33 mg/kg, respectively. Whereas for the scaled LHD, MHD, and HHD, the estimated median values ranged from nearly 0.01 to 2.6 mg/kg (Supplementary Figure S3).

Simulated maximum concentrations of AuNPs in target tissues or organs (liver, kidney, venous plasma, and rest of body) within 24 h after low, medium, and high IV administration can be well depicted with LN distributions (Figure 4(D–O)). For humans directly receiving LAD, MAD, and HAD, the maximum internal concentrations were observed in venous plasma with geometric means (GMs) of LN distribution estimated to be around 0.9, 10.8 and

418.8 $\mu\text{g/ml}$, respectively (Figure 4(E,I,M)). Whereas for people receiving the high scaled dosing level, maximum concentration occurred at 24 h in liver with GM and geometric standard deviation (GSD) estimated to be 45.3 $\mu\text{g/g}$ and 1.1, respectively (Supplementary Figure S3). The lowest C_{max} were found in rest of body among all selected tissues or organs with GMs estimated to be around 0.1, 0.8 and 4.6 $\mu\text{g/g}$, respectively, after receiving LAD, MAD, and HAD (Figure 4(G,K,O)). A similar trend of distribution of internal concentrations in rest of body can be found in humans receiving various scaled HDs with GMs estimated to be around 0.01–1.5 $\mu\text{g/g}$ (Supplementary Figure S3). Comparing all distribution profiles, medium and high dosage-based internal concentration distribution profiles more likely followed a normal rather than lognormal distribution with GSDs approximating 1 (Figure 4(H–O) and Supplementary Figure S3).

Risk estimation

By linking maximum internal concentrations estimated from the human PBPK model with

Table 1. Fitted parameters (mean \pm SE) of the three- or four-parameter Hill model for reconstructing the relationship between exposure concentration and fractional cell death.

Human cell types	Size/surface coating of AuNPs	E_{\min}	E_{\max}^a	EC_{50}	n	r^2
Hepatocytes	40 nm; BPEI-HP	0.00001 \pm 0.03	1	273.30 \pm 23.36***	2.47 \pm 0.45***	0.95***
	80 nm; BPEI-HP	0.007 \pm 0.004	1	394.66 \pm 5.45***	4.22 \pm 0.28***	0.99***
	40 nm; BPEI	0.03 \pm 0.02	1	185.01 \pm 7.89***	6.16 \pm 1.86**	0.94***
HUVEC	80 nm; BPEI	0.02 \pm 0.04	1	210.07 \pm 15.52***	2.46 \pm 0.57***	0.90***
	40 nm; BPEI	0.006 \pm 0.03	1	78.14 \pm 1.68***	5.30 \pm 0.60***	0.96***
	80 nm; BPEI	0.008 \pm 0.04	1	81.21 \pm 2.30***	4.53 \pm 0.67***	0.94***
HRPTEC	40 nm; PEG	0.00001 \pm 0.05	0.26	83.63 \pm 23.37**	1.58 \pm 1.01	0.43*
	40 nm; BPEI	0.00002 \pm 0.04	1	68.20 \pm 4.39***	2.26 \pm 0.27***	0.98***
Keratinocytes	40 nm; BPEI	0.02 \pm 0.02	1	70.42 \pm 2.25***	3.90 \pm 0.34***	0.98***
	80 nm; BPEI	0.09 \pm 0.04*	1	62.37 \pm 5.47***	2.77 \pm 0.60***	0.91***
PMNs	20 nm	0.26 \pm 0.03***	0.60	35.17 \pm 33.14 ^b	0.29 \pm 0.13*	0.63***
	70 nm	0.35 \pm 0.02***	0.83	249.45 \pm 112.23*	0.47 \pm 0.13**	0.81***

BPEI: branched polyethylenimine; PEG: polyethylene glycol; E_{\min} and E_{\max} : minimum and maximum fraction of cell death; EC_{50} : exposure concentration leading to half maximum fractional cell death ($\mu\text{g/ml}$); HP: human plasma protein; n : Hill coefficient; r^2 : coefficient of determination.

^a $E_{\max} = 1$ or $E_{\max} < 1$ obtains the three- or four-parameter Hill model, respectively.

^bThe large standard deviation was due to the dataset used. The observed maximal cell death rate was 60%, thus there was a great uncertainty from 60% to 100% cell death.

* $p < 0.05$; ** $p < 0.01$; *** $p < 0.001$.

constructed *in vitro* dose–response models, the human exposure risk to AuNPs with different sizes and surface coatings can be estimated. Specifically, the results showed that there was a 50% risk probability for people receiving low and medium non-scaled AuNP IV doses to have more than 0.001–3.4, 0.02–1.0, 0.003–0.1, and 1.7–8.9% cell death in hepatocytes (Figure 5(A,B)), HUVEC (Figure 5(D,E,G,H)), HRPTEC (Figure 5(J,K)), and keratinocytes (Figure 5(M,N)), respectively. Only receiving high non-scaled dosages of AuNP-BPEI would give rise to particularly high percentages of cell death ranging from around 53–88, 100, and 95–98 for hepatocytes, HUVEC, and HRPTEC, respectively, with all probable risk probabilities being considered (Figure 5(C,F,L)). On the other hand, exposure to the highest scaled dosages of AuNP-BPEI and AuNP-PEG would induce only <10% cell death, suggesting none to minimal toxicity if incorporating animal-derived HDs based on allometric scaling to the human PBPK model (Supplementary Figure S4).

Human equivalent dose estimates

Supplementary Table S5 summarizes the *in vitro* exposure concentrations causing 5% and 10% maximum cell death in four human cell types. The EC_5 -derived HED estimates ranged 1.0–7.4 and 2.5–21.1 mg/kg for hepatocytes exposed to bare AuNP-BPEI and AuNP-BPEI-HP, respectively; whereas the EC_{10} -derived HED estimates for hepatocytes exposed to bare AuNP-BPEI and AuNP-BPEI-HP ranged 2.1–8.0

and 4.2–43.1 mg/kg, respectively (Figure 6(A)). Furthermore, HEDs associated with PODs derived from animal studies were estimated to be 0.5, 1.4 and 0.005 mg/kg based on reported NOAEL and LOAEL for mice and LOAEL for rats, respectively (Figure 6(A)).

Besides the target organ liver, this study also estimated HEDs based on the internal concentrations in other tissues (i.e. venous plasma and kidney) as depicted in Figure 6(C). The EC_5 - and EC_{10} -derived HEDs were estimated to be in the ranges of 2.7–4.1 and 3.3–4.6 mg/kg, respectively, based on HUVEC, and were 3.0–7.2 and 3.9–8.8 mg/kg, respectively, based on HRPTEC exposed to bare AuNP-BPEI. In addition, for HUVEC exposed to bare AuNP-PEG, the EC_5 - and EC_{10} -derived HED estimates ranged from 1.0 to 4.5 and 2.5 to 8.2, respectively (Figure 6(C)).

Discussion

The present study reconstructed *in vitro* dose–response relationships for different types of AuNPs in selective human cells derived from different tissues or organs of healthy individuals. We also characterized AuNP external and internal exposure dosimetry based on a wide range of reported doses used in animal studies and converted into human-equivalent doses. Our analyses suggest that for people receiving frequently applied IV doses of AuNPs from animal studies (low-to-medium range in our analysis), no or limited cytotoxicity (relative to baseline cell death) might be observed in vascular

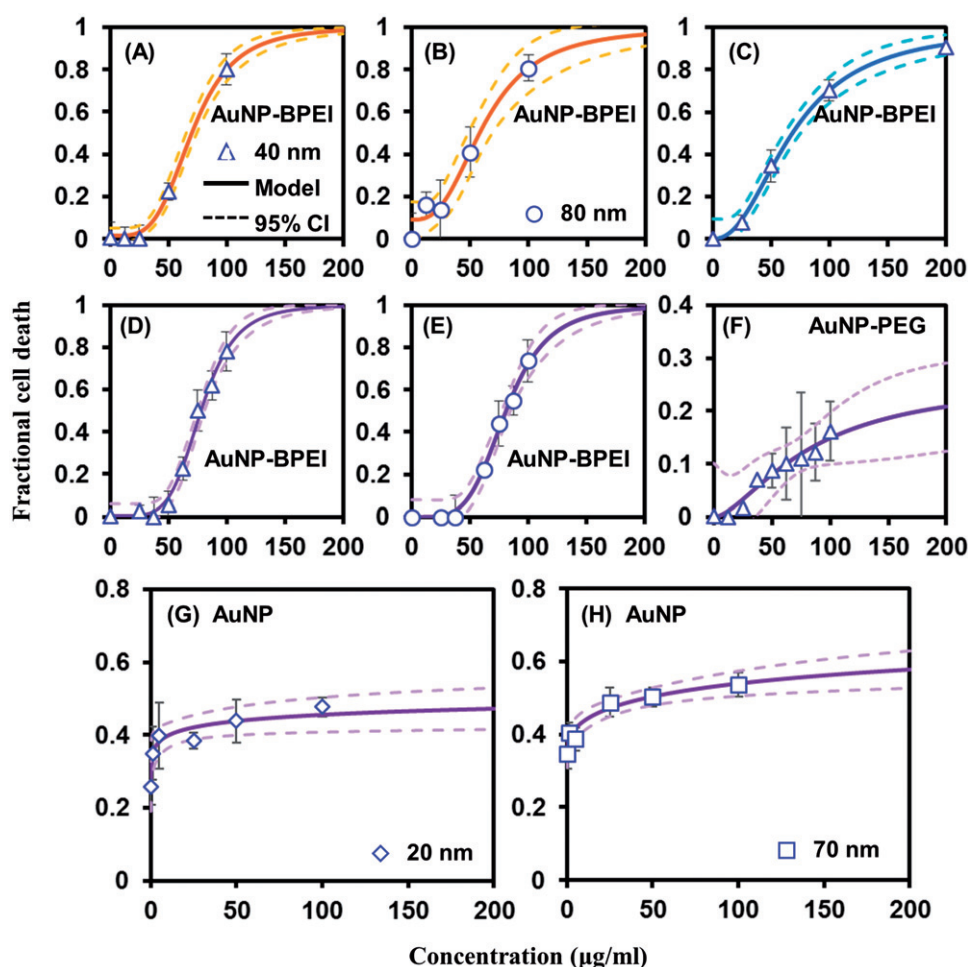


Figure 3. Fitted relationships between the concentrations of AuNPs and fractional cell death for keratinocytes (A and B), HRPTEC (C), HUVEC (D–F), and PMNs (G and H) exposed to different sizes and types of AuNPs.

endothelial, liver, kidney, or skin cells. Yet, people should be aware of that extremely high cytotoxicity could occur in target organs or tissues if one received high dosages associated with those reported in rodents, even though very few animal studies have used the high dose range.

The lowest *in vitro* response-derived mean HED estimate of 2.7 mg/kg was around three times higher than median MAD estimate of 0.8 and comparable to median HHD estimate of 2.6 mg/kg, respectively. These results suggest that the commonly used doses in animal studies that show diagnostic, anticancer, or other therapeutic effects, if the same doses are used in humans, may cause minimal cytotoxicity. The estimated HED derived from rat study based on different toxicity endpoint (i.e. change in gene expression in liver) was 0.005 mg/kg, which is lower than the median LHD of 0.01 mg/kg. Together, these results suggest that while substantial cytotoxicity is unlikely after receiving frequently

applied IV dosages of AuNPs, other subtle changes such as changes in the gene expression should not be ignored.

Even after decades of development, whether AuNPs are biocompatible and safe remains controversial. Numerous studies have reported non-toxicity or low toxicity of AuNPs (Xu et al. 2008; Simpson et al. 2013; Mannerström et al. 2016), findings consistent with the present study. Specifically, Mannerström et al. (2016) investigated cellular toxicity in mouse BALB/c 3T3 fibroblasts, rat NR8383 macrophages, as well as human U937 monocytes exposed to 13 nm citrate-coated AuNPs (0–6 µg/ml) and revealed no significant cytotoxicity. A recent *in vivo* study showed that 1.2 nm glutathione-coated AuNPs were biocompatible and had low immunogenicity for exposure concentration up to 60 µM in 200 µl injection per mouse (0.15 mg/kg) (Simpson et al. 2013). In particular, Xu et al. (2008) demonstrated that AuNPs (4–60 nm) did not significantly

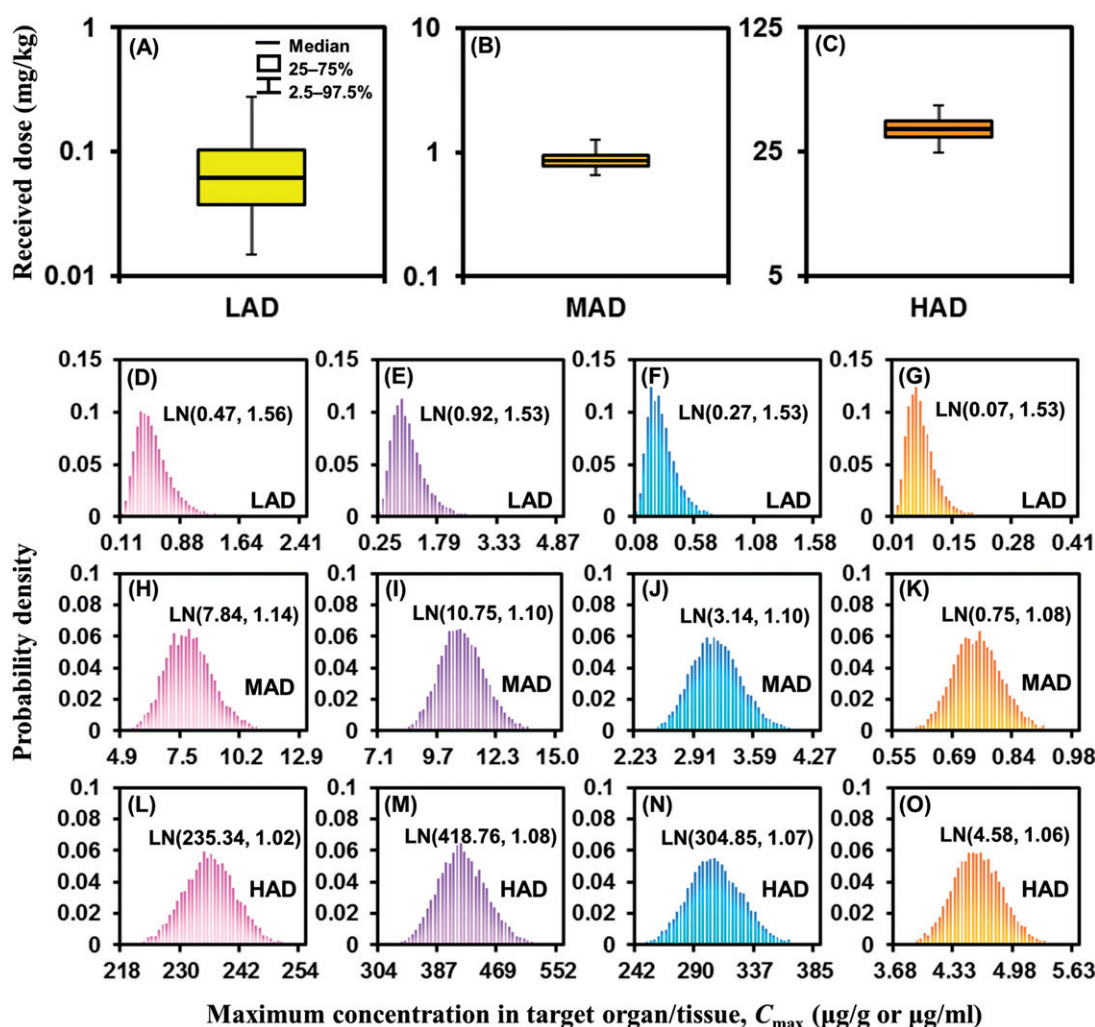


Figure 4. PBPK model-predicted internal organ concentrations of AuNPs. (A–C) represent low, medium, and high animal doses (LAD, MAD, and HAD), respectively. (D–O) represent maximum internal concentrations in liver (pink) (D,H,L), venous plasma (purple) (E,I,M), kidney (blue) (F,J,N), and skin (orange) (G,K,O) estimated from human AuNP-PBPK model within 24 h after intravenous injection with LAD, MAD, and HAD, respectively.

decrease the viability of human HeLa S3 cells at exposure concentration up to 1000 $\mu\text{g/ml}$.

Jo et al. (2015) reported that although short-term AuNP toxicity was not observed in both *in vitro* (human intestinal epithelial cells, INT-407) and *in vivo* (rats) studies at a high exposure concentration or dosage of 13 $\mu\text{g/ml}$ and mg/kg , potential toxicity may occur in a long-term cell proliferation assay (measured with colony-forming ability). Chen et al. (2009) suggested the long-term toxicity in mice receiving 8–37 nm AuNPs intraperitoneally at a dose of 8 mg/kg/week for 1 month with most of the mice dying before 21 days. Not dramatic but significant toxicity was demonstrated by two *in vivo* studies in mice with inflammation in the liver (7-day exposure) (Cho et al. 2009) and in rats with changes in the

expression of hepatic genes related to detoxification, lipid metabolism, and cell cycle effects (2-month exposure) (Balasubramanian et al. 2010), respectively. While our study suggests that minimal or no toxicity may occur within 24 h after single IV exposure of commonly applied dosing levels in rodent studies, the potential toxicity after repeated or long-term exposure cannot be deemphasized and is a subject of our future studies.

None to low toxicity associated with commonly applied animal dosing levels indicated by our analyzes might result partly because of diluted internal concentrations in target tissues/organs associated with PBPK model involving biodistribution and excretion or modulated biological responses by AuNPs with HP corona formation. Previous studies

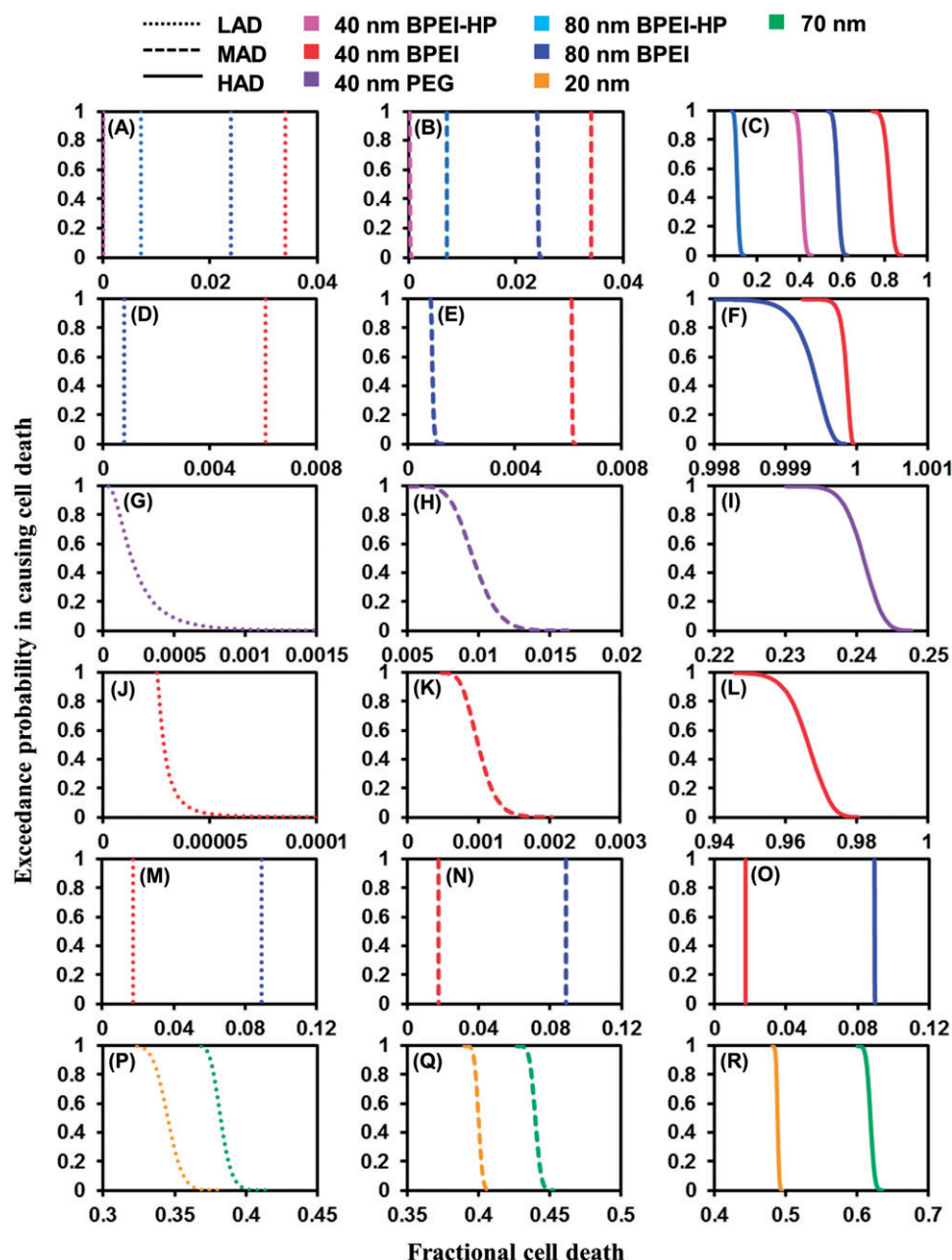


Figure 5. Exceedance risk profiles of internal concentration-associated cell death fractions in hepatocytes (A–C), HUVEC (D–I), HRPTEC (J–L), keratinocytes (M–O), and PMNs (P–R) at various non-scaled intravenous doses.

have demonstrated that AuNPs with HP corona formation could considerably attenuate cytotoxicity, proinflammatory cytokine expression, catalytic activity of cytochrome P450, and reactive oxygen/reactive nitrogen species production (Casals et al. 2010; Choi et al. 2017; Parveen et al. 2017). Following different routes of administration, NPs will be covered with different protein coronas, resulting in different biodistribution patterns and differential toxicity in varied species (Sahneh et al. 2015; Kreyling et al. 2017a, 2017b, 2017c). In addition, measured

baseline values in cell death assessment may vary between different human cell types, e.g. between PMNs (Noël et al. 2016) and HUVEC (Chandran et al. 2017).

It is worthy of note that currently there is no consensus on the best method for scaling or selecting the first dose of AuNPs in humans. With potential implications of AuNPs to future therapeutic nanomedicine in humans, this study scaled frequently applied rodent dosages into human-correlated dosages (Sharma and McNeill 2009). Based

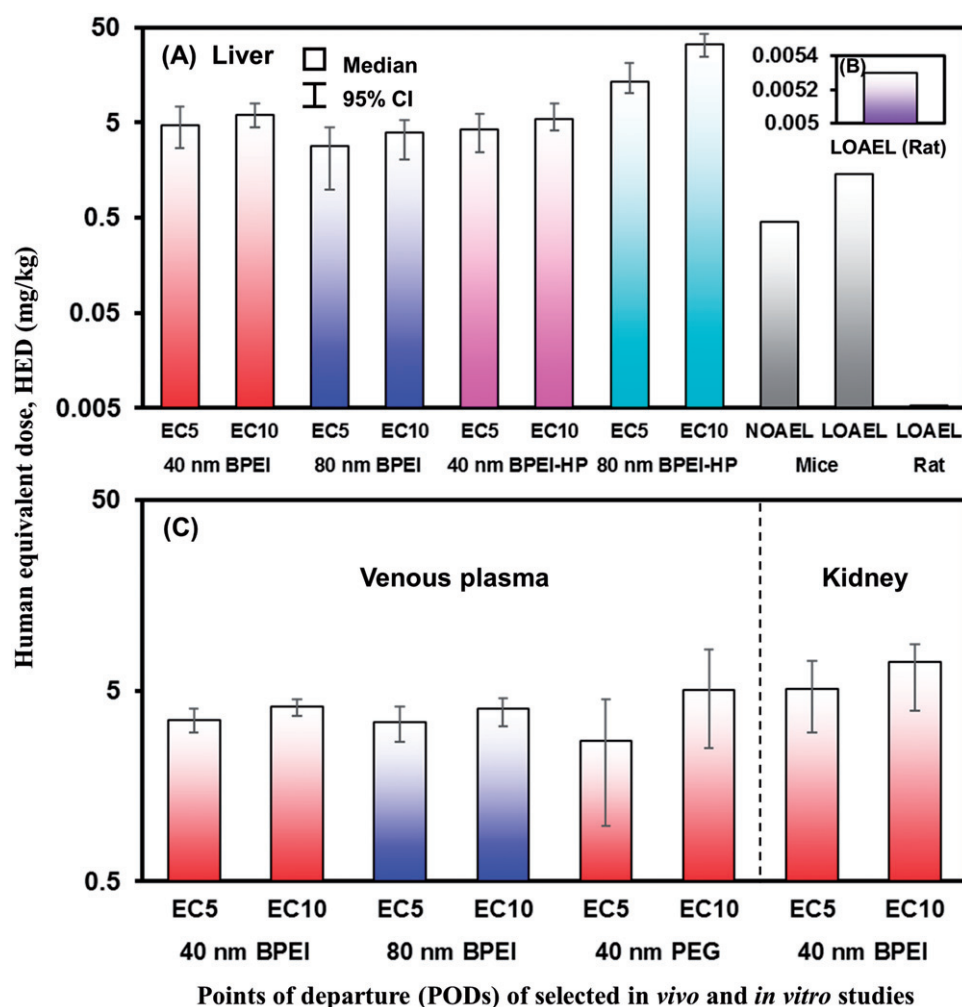


Figure 6. Human equivalent doses estimated through human AuNP-PBPK model based on points of departure, including EC_5 and EC_{10} estimated from *in vitro* as well as NOAEL and/or LOAEL from *in vivo* experimental data in liver (A), venous plasma and kidney (C). (B) Enhanced inset of (A).

on this scaling method, our analyzed results suggest that even for people receiving the highest IV dosing levels would result in minimal cytotoxicity in hepatocytes, HUVEC, HRPTEC, and keratinocytes (Supplementary Figure S4). In comparison, extremely high cell death fraction might occur in people intravenously administered with the highest animal dosages of bare AuNP-BPEI. Yet, exposure to AuNPs with varied physicochemical characteristics, e.g. bare AuNP-PEG versus bare AuNP-BPEI, would induce differential cytotoxicity. Even though this study implies that great cytotoxicity might occur in people receiving high animal dose, none to minimal toxicity were reported from rodent studies applying high doses of AuNP-PEG or glutathione-coated AuNPs (James et al. 2007; Wong et al. 2013). Other potential toxicity effects associated with different cell types, exposure concentration, and duration by

different AuNPs or different routes of exposure might exist in various species and need to be explored in future studies.

To the best of our knowledge, this is the first study integrating *in vitro* dose-response relationships based on different healthy human cell types, a validated human PBPK model, probabilistic risk assessment method, and adequate exposure reconstruction to quantitatively assess the potential toxicity risks induced by AuNPs. Recently, additional NP-related studies have incorporated PBPK modeling approach to estimate environmental and/or occupational exposure with the intention to implicate potential risk (Bachler et al. 2013, 2015; Mahapatra et al. 2015). Nevertheless, none of these studies implemented a probabilistic approach incorporating physiologically based external-to-internal dosimetric model (i.e. PBPK model) and various

toxicity endpoints to derive different PODs for biological responses in animals and humans, which is an essential element in conducting environmental and occupational risk assessment either for ecosystem or human health (Bhatt and Tripathi 2011; Kuempel et al. 2015). Stated differently, earlier studies were based solely on toxicokinetic analyzes without integrating a toxicodynamic response.

One common limitation in risk assessment when integrating multiple data sources and modeling frameworks is the uncertainty in risk estimates. This limitation also applies to the present study. To reduce uncertainty, this study employed a verified human PBPK model to describe external-to-internal dosimetry relationship. Regarding dose–response relationship, the analyzes were mostly based on *in vitro* toxicity data collected from the same laboratory that had very similar experimental designs and conditions, which would help reduce uncertainty. Additionally, by implementing a Bayesian-based probabilistic risk assessment approach, we were able to take the parameter variability into account to reduce potential uncertainty. Future studies that use the same NPs to conduct *in vitro* and *in vivo* toxicity, as well as PBPK modeling studies are needed in order to further reduce uncertainty in our analysis.

This present study had implemented the ISDD model (Hinderliter et al. 2010) to estimate the deposited fractions of AuNPs at different time points after exposure based on the experimental condition described in Choi et al. (2017) (Supplementary Table S2). By integrating *in vitro* time course data with PBPK and ISDD models, differential *in vivo* cytotoxicity endpoints induced by AuNPs at different exposure time scales and different levels of biology (i.e. cellular, organ, and tissue levels) could be characterized and compared with endpoints observed after *in vitro* exposure. However, in order to fully integrate the PBPK model with ISDD model, it is necessary to develop a more detailed mechanistic model that can simulate the concentrations of NPs at both the organ and individual cellular levels, including intracellular level. Once such multi-scale models are established, it would be possible to integrate *in vitro* and *in vivo* transcriptomics, genomics, metabolomics, as well as other toxicity time course data with the ISDD/PBPK models to conduct IVIVE and to gain more insights into the potential toxicity of NPs. In this regard,

recent studies have demonstrated that it is possible to link genomics or transcriptomics data to whole-body PBPK models by integrating data from multiple sources to study mechanisms of chemical-induced toxicities (Andersen et al. 2017; Maldonado et al. 2017; Cordes et al. 2018). Our recent studies have determined the effects of AuNPs on the expression of multiple genes related to different functional pathways in different cells (Chandran et al. 2017; Choi et al. 2017). Further studies are warranted to determine the effects of AuNPs on the genomics, transcriptomics, or metabolomics in target cells or tissues, and to develop the proposed multi-scale model to better determine the potential risk of AuNPs and to elucidate the potential toxic mechanisms.

This study showed that *in vitro*-associated HEDs were higher than those derived from *in vivo* rodent studies. However, these HEDs are not directly comparable because the *in vitro* toxicity endpoint (e.g. cell death) is significantly different from the sublethal *in vivo* toxicity endpoints (e.g. gene expression changes in liver) and the AuNPs used in our earlier *in vitro* studies are different from those used in the selected *in vivo* studies. More *in vivo* as well as *in vitro* studies targeting the same biological response using the same type of AuNPs are urgently needed to develop and verify appropriate conversion factors with implications to interspecies extrapolation or IVIVE and to further assess the potential risk for AuNPs (Teeguarden et al. 2007; Riviere 2013; Li et al. 2017b). A PBPK model established based upon IV pharmacokinetic data may not be a suitable surrogate approach to describe pharmacokinetics after inhalational and oral uptakes (Kreyling et al. 2017a, 2017b, 2017c). Therefore, a PBPK model incorporating multiple exposure pathways is necessary to bridge environmental, occupational, or medical exposure doses and the probable magnitude in biological responses to systemically characterize potential exposure risks of AuNPs (Hirn et al. 2011; Schleh et al. 2012; Johnston et al. 2013; Kreyling et al. 2014; Riviere 2013; Bachler et al. 2013, 2015).

Conclusions

We applied a probabilistic risk assessment approach to systemically characterize AuNP exposure risks in

humans by associating a validated human PBPK model with well-established *in vitro* dose–response relationships. This work suggests potentially none to mild nanotoxicity for people intravenously administered with various AuNP dosages that were equivalent to the allometrically scaled or non-scaled commonly used doses in rodent studies. Based on exposure reconstructions from *in vitro* to *in vivo* extrapolation and from animal to human extrapolation, this study provides recommended AuNP administration doses that prevent people from toxicity endpoints. This study suggests that it is critical to adequately derive human equivalent doses from doses used in rodent studies for future clinical and risk assessment implications. Our computational approach provides new insights into AuNP toxicity prediction and safety evaluation in humans, an approach that could also be applied to other types of NPs.

Acknowledgements

We would like to thank Drs Ronette Gehring, Majid Jaber-Douraki and Miao Li in the ICCM at Kansas State University for helpful discussions. We also would like to acknowledge our NICKS colleagues Dr Parwathy Chandran, Dr Yang Li, Dr Kyoungju Choi, and Dr Maria T. Ortega whose previously published *in vitro* toxicity data were essential for our analysis.

Disclosure statement

The authors declare no conflict of interest.

Funding

This work was supported by The Kansas Bioscience Authority funds to the Institute of Computational Comparative Medicine (ICCM) and Nanotechnology Innovation Center of Kansas State (NICKS), the K-State Mentoring Fellowship, and the New Faculty Start-up funds at Kansas State University.

ORCID

Yi-Hsien Cheng  <https://orcid.org/0000-0002-4314-9732>

Jim E. Riviere  <http://orcid.org/0000-0001-8412-9650>

Nancy A. Monteiro-Riviere  <http://orcid.org/0000-0002-0132-0861>

Zhoumeng Lin  <http://orcid.org/0000-0002-8731-8366>

References

Andersen, M.E., M. B. Black, J. L. Campbell, S. N. Pendse, H. J. Clewell, III, L. H. Pottenger, J. S. Bus, et al. 2017.

- "Combining Transcriptomics and PBPK Modeling Indicates a Primary Role of Hypoxia and Altered Circadian Signaling in Dichloromethane Carcinogenicity in Mouse Lung and Liver." *Toxicology and Applied Pharmacology* 332: 149–158.
- Arvizo, R. R., S. Bhattacharyya, R. A. Kudgus, K. Giri, R. Bhattacharya, and P. Mukherjee. 2012. "Intrinsic Therapeutic Applications of Noble Metal Nanoparticles: Past, Present and Future." *Chemical Society Reviews* 41 (7): 2943–2970.
- Bachler, G., N. von Goetz, and K. Hungerbühler. 2013. "A Physiologically based Pharmacokinetic Model for Ionic Silver and Silver Nanoparticles." *International Journal of Nanomedicine* 8:3365–3382.
- Bachler G, von Goetz N, Hungerbuhler K. 2015. "Using Physiologically based Pharmacokinetic (PBPK) Modeling for Dietary Risk Assessment of Titanium Dioxide (TiO₂) Nanoparticles." *Nanotoxicology* 9 (3): 373–380.
- Balasubramanian, S. K., J. Jittiwat, J. Manikandan, C. N. Ong, L. E. Yu, and W. Y. Ong. 2010. "Biodistribution of Gold Nanoparticles and Gene Expression Changes in the Liver and Spleen after Intravenous Administration in Rats." *Biomaterials* 31 (8): 2034–2042.
- Bhatt, I., and B. N. Tripathi. 2011. "Interaction of Engineered Nanoparticles with Various Components of the Environment and Possible Strategies for their Risk Assessment." *Chemosphere* 82 (3):308–317.
- Bois, F. Y., M. Jamei, and H. J. Clewell. 2010. "PBPK Modelling of Inter-individual Variability in the Pharmacokinetics of Environmental Chemicals." *Toxicology* 278 (3): 256–267.
- Casals, E., T. Pfaller, A. Duschl, G. J. Oostingh, and V. Puentes. 2010. "Time Evolution of the Nanoparticle Protein Corona." *ACS Nano* 4 (7): 3623–3632.
- Chandran, P., J. E. Riviere, and N. A. Monteiro-Riviere. 2017. "Surface Chemistry of Gold Nanoparticles Determines the Biocorona Composition Impacting Cellular Uptake, Toxicity and Gene Expression Profiles in Human Endothelial Cells." *Nanotoxicology* 11 (4): 507–519.
- Chen, Y. S., Y. C. Hung, I. Liao, and G. S. Huang. 2009. "Assessment of the In Vivo Toxicity of Gold Nanoparticles." *Nanoscale Research Letters* 4 (8): 858–864.
- Cheng, Y.-H., Y.-J. Lin, S.-H. You, Y.-F. Yang, C. M. How, Y.-T. Tseng, W.-Y. Chen, and C.-M. Liao. 2016. "Assessing Exposure Risks for Freshwater Tilapia Species Posed by Mercury and Methylmercury." *Ecotoxicology* 25 (6): 1181–1193.
- Cho, W.-S., M. Cho, J. Jeong, M. Choi, H.-Y. Cho, B. S. Han, S. H. Kim, et al. 2009. "Acute Toxicity and Pharmacokinetics of 13 nm-Sized PEG-Coated Gold Nanoparticles." *Toxicology and Applied Pharmacology* 236 (1): 16–24.
- Choi, K., J. E. Riviere, and N. A. Monteiro-Riviere. 2017. "Protein Corona Modulation of Hepatocyte Uptake and Molecular Mechanisms of Gold Nanoparticle Toxicity." *Nanotoxicology* 11 (1): 64–75.
- Cohen, J. M., J. G. Teeguarden, and P. Demokritou. 2014. "An Integrated Approach for the In Vitro Dosimetry of

- Engineered Nanomaterials." *Particle and Fibre Toxicology* 11:20.
- Cordes, H., C. Thiel, V. Baier, L. M. Blank, and L. Kuepfer. 2018. "Integration of Genome-Scale Metabolic Networks into Whole-Body PBPK Models Shows Phenotype-Specific Cases of Drug-Induced Metabolic Perturbation." *NPJ Systems Biology and Applications* 4:10.
- DeLoid, G. M., J. M. Cohen, G. Pyrgiotakis, and P. Demokritou. 2017. "Preparation, Characterization, and In Vitro Dosimetry of Dispersed, Engineered Nanomaterials." *Nature Protocols* 12 (2): 355–371.
- EPA. 2012. *Benchmark Dose Technical Guidance*. Washington, DC: U.S. Environmental Protection Agency (EPA). https://www.epa.gov/sites/production/files/2015-01/documents/benchmark_dose_guidance.pdf.
- EPA. 2014. *Probabilistic Risk Assessment to Inform Decision Making: Frequently Asked Questions*. Washington, DC: U.S. EPA. <https://www.epa.gov/sites/production/files/2014-11/documents/raf-pra-faq-final.pdf>.
- Hinderliter, P. M., K. R. Minard, G. Orr, W. B. Chrisler, B. D. Thrall, J. G. Pounds, and J. G. Teeguarden. 2010. "ISDD: A Computational Model of Particle Sedimentation, Diffusion and Target Cell Dosimetry for In Vitro Toxicity Studies." *Particle and Fibre Toxicology* 7 (1): 36.
- Hirn S., M. Semmler-Behnke, C. Schleh, A. Wenk, J. Lipka, M. Schäffler, S. Takenaka, et al. 2011. "Particle Size-Dependent and Surface Charge-Dependent Biodistribution of Gold Nanoparticles after Intravenous Administration." *European Journal of Pharmaceutics and Biopharmaceutics* 77 (3): 407–416.
- Jain, S., D. G. Hirst, and J. M. O'Sullivan. 2012. "Gold Nanoparticles as Novel Agents for Cancer Therapy." *British Journal of Radiology* 85 (1010): 101–113.
- James, W. D., L. R. Hirsch, J. L. West, P. D. O'Neal, and J. D. Payne. 2007. "Application of INAA to the Build-up and Clearance of Gold Nanoshells in Clinical Studies in Mice." *Journal of Radioanalytical and Nuclear Chemistry* 271 (2): 455–459.
- Jo, M. R., S. H. Bae, M. R. Go, H. J. Kim, Y. G. Hwang, and S. J. Choi. 2015. "Toxicity and Biokinetics of Colloidal Gold Nanoparticles." *Nanomaterials (Basel)* 5 (2): 835–850.
- Johnston, H., G. Pojana, S. Zuin, N. R. Jacobsen, P. Möller, S. Loft, M. Semmler-Behnke, et al. 2013. Engineered Nanomaterial Risk. Lessons Learnt from Completed Nanotoxicology Studies: Potential Solutions to Current and Future Challenges." *Critical Reviews in Toxicology* 43 (1): 1–20.
- Khlebtsov, N., and L. Dykman. 2011. "Biodistribution and Toxicity of Engineered Gold Nanoparticles: A Review of In Vitro and In Vivo Studies." *Chemical Society Reviews* 40 (3): 1647–1671.
- Kreyling W. G., S. Hirn, W. Möller, C. Schleh, A. Wenk, G. Celik, J. Lipka, et al. 2014. "Air-Blood Barrier Translocation of Tracheally Instilled Gold Nanoparticles Inversely Depends on Particle Size." *ACS Nano* 8 (1): 222–233.
- Kreyling, W. G., U. Holzwarth, N. Haberl, J. Kozempel, S. Hirn, A. Wenk, et al. 2017a. "Quantitative Biokinetics of Titanium Dioxide Nanoparticles after Intravenous Injection in Rats: Part 1." *Nanotoxicology* 11: 434–442.
- Kreyling, W. G., U. Holzwarth, N. Haberl, J. Kozempel, A. Wenk, S. Hirn, et al. 2017c. "Quantitative Biokinetics of Titanium Dioxide Nanoparticles after Intratracheal Instillation in Rats: Part 3." *Nanotoxicology* 11: 454–464.
- Kreyling, W. G., U. Holzwarth, C. Schleh, J. Kozempel, A. Wenk, N. Haberl, et al. 2017b. "Quantitative Biokinetics of Titanium Dioxide Nanoparticles after Oral Application in Rats: Part 2." *Nanotoxicology* 11: 443–453.
- Kuempel, E. D., L. M. Sweeney, J. B. Morris, and A. M. Jarabek. 2015. "Advances in Inhalation Dosimetry Models and Methods for Occupational Risk Assessment and Exposure Limit Derivation." *Journal of Occupational and Environmental Hygiene* 12(suppl 1): S18–S40.
- Li, M., R. Gehring, J. E. Riviere, and Z. Lin. 2017a. "Development and Application of a Population Physiologically based Pharmacokinetic Model for Penicillin G in Swine and Cattle for Food Safety Assessment." *Food and Chemical Toxicology* 107: 74–87.
- Li, M., P. Zou, K. Tyner, and S. Lee. 2017b. "Physiologically Based Pharmacokinetic (PBPK) Modeling of Pharmaceutical Nanoparticles." *AAPS Journal* 19: 26–42.
- Li, Y., and N. A. Monteiro-Riviere. 2016. "Mechanisms of Cell Uptake, Inflammatory Potential and Protein Corona Effects with Gold Nanoparticles." *Nanomedicine (London)* 11 (24): 3185–3203.
- Lin, Z., M. Jaber-Douraki, C. He, S. Jin, R. S. H. Yang, J. W. Fisher, J. E. Riviere, et al. 2017. "Performance Assessment and Translation of Physiologically based Pharmacokinetic Models from acslX™ to Berkeley Madonna™, MATLAB®, and R Language: Oxytetracycline and Gold Nanoparticles as Case Examples." *Toxicological Sciences*, 158 (1): 23–35.
- Lin, Z., N. A. Monteiro-Riviere, R. Kannan, and J. E. Riviere. 2016a. "A Computational Framework for Interspecies Pharmacokinetics, Exposure and Toxicity Assessment of Gold Nanoparticles." *Nanomedicine (London)* 11: 107–119.
- Lin, Z., N. A. Monteiro-Riviere, and J. E. Riviere. 2015. "Pharmacokinetics of Metallic Nanoparticles." *Wiley Interdisciplinary Reviews: Nanomedicine Nanobiotechnology* 7 (2): 189–217.
- Lin, Z., N. A. Monteiro-Riviere, and J. E. Riviere. 2016b. "A Physiologically based Pharmacokinetic Model for Polyethylene Glycol-Coated Gold Nanoparticles of Different Sizes in Adult Mice." *Nanotoxicology* 10: 162–172.
- Mahapatra, I., T. Y. Sun, J. R. A. Clark, P. J. Dobson, K. Hungerbuehler, R. Owen, B. Nowack, et al. 2015. "Probabilistic Modelling of Prospective Environmental Concentrations of Gold Nanoparticles from Medical Applications as a Basis for Risk Assessment." *Journal of Nanobiotechnology* 13: 93.
- Maldonado, E. M., V. Leoncikis, C. P. Fisher, J. B. Moore, N. J. Plant, and A. M. Kierzek. 2017. "Integration of Genome Scale Metabolic Networks and Gene Regulation of Metabolic Enzymes with Physiologically Based Pharmacokinetics." *CPT: Pharmacometrics & Systems Pharmacology* 6 (11): 732–746.

- Mannerström, M., J. Zou, T. Toimela, I. Pyykkö, and T. Heinonen. 2016. "The Applicability of Conventional Cytotoxicity Assays to Predict Safety/Toxicity of Mesoporous Silica Nanoparticles, Silver and Gold Nanoparticles and Multi-Walled Carbon Nanotubes." *Toxicology In Vitro* 37: 113–120.
- Monteiro-Riviere, N. A., A. O. Inman, and L. W. Zhang. 2009. "Limitations and Relative Utility of Screening Assays to Assess Engineered Nanoparticle Toxicity in a Human Cell Line." *Toxicology and Applied Pharmacology* 234 (2): 222–235.
- Nair, A. B., and S. A. Jacob. 2016. "A Simple Practice Guide for Dose Conversion Between Animals and Human." *Journal of Basic and Clinical Pharmacy* 7 (2): 27–31.
- Noël, C., J. C. Simard, and D. Girard. 2016. "Gold Nanoparticles Induce Apoptosis, Endoplasmic Reticulum Stress Events and Cleavage of Cytoskeletal Proteins in Human Neutrophils." *Toxicology In Vitro* 31: 12–22.
- NRC (National Research Council) 2009. *Science and Decisions: Advancing Risk Assessment*. Washington, DC: The National Academies Press. <https://www.nap.edu/catalog/12209/science-and-decisions-advancing-risk-assessment>.
- Ortega, M. T., J. E. Riviere, K. Choi, and N. A. Monteiro-Riviere. 2017. "Biocorona Formation on Gold Nanoparticles Modulates Human Proximal Tubule Kidney Cell Uptake, Cytotoxicity and Gene Expression." *Toxicology In Vitro* 42: 150–160.
- Parveen, R., T. N. Shamsi, and S. Fatima. 2017. "Nanoparticles-Protein Interaction: Role in Protein Aggregation and Clinical Implications." *International Journal of Biological Macromolecules* 94 (Pt A): 386–395.
- Pernodet, N., X. Fang, Y. Sun, A. Bakhtina, A. Ramakrishnan, J. Sokolov, A. Ulman, et al. 2006. "Adverse Effects of Citrate/Gold Nanoparticles on Human Dermal Fibroblasts." *Small* 2 (6): 766–773.
- Riviere, J. E. 2013. "Of Mice, Men and Nanoparticle Biocoronas: Are In Vitro to In Vivo Correlations and Interspecies Extrapolations Realistic?" *Nanomedicine (London)* 8 (9): 1357–1359.
- Sahneh, F. D., C. M. Scoglio, N. A. Monteiro-Riviere, and J. E. Riviere. 2015. "Predicting the Impact of Biocorona Formation Kinetics on Interspecies Extrapolations of Nanoparticle Biodistribution Modeling." *Nanomedicine (London)* 10 (1): 25–33.
- Schleh, C., M. Semmler-Behnke, J. Lipka, A. Wenk, S. Hirn, M. Schäffler, G. Schmid, et al. 2012. "Size and Surface Charge of Gold Nanoparticles Determine Absorption Across Intestinal Barriers and Accumulation in Secondary Target Organs after Oral Administration." *Nanotoxicology* 6 (1): 36–46.
- Sharma, V., and J. H. McNeill. 2009. "To Scale or Not to Scale: The Principles of Dose Extrapolation." *British Journal of Pharmacology* 157 (6): 907–921.
- Shi, Z., S. K. Chapes, D. Ben-Arieh, and C. H. Wu. 2016. "An Agent-Based Model of a Hepatic Inflammatory Response to *Salmonella*: A Computational Study under a Large Set of Experimental Data." *PLoS One* 11 (8): e0161131.
- Simpson, C. A., K. J. Salleng, D. E. Cliffler, and D. L. Feldheim. 2013. "In Vivo Toxicity, Biodistribution, and Clearance of Glutathione-Coated Gold Nanoparticles." *Nanomedicine* 9 (2): 257–263.
- Teeguarden, J. G., P. M. Hinderliter, G. Orr, B. D. Thrall, and J. G. Pounds. 2007. "Particokinetics In Vitro: Dosimetry Considerations for In Vitro Nanoparticle Toxicity Assessments." *Toxicological Sciences* 95 (2): 300–312.
- Westmeier, D., R. H. Stauber, and D. Docter. 2016. "The Concept of Bio-Corona in Modulating the Toxicity of Engineered Nanomaterials (ENM)." *Toxicology and Applied Pharmacology* 299: 53–57.
- Wong, O. A., R. J. Hansen, T. W. Ni, C. L. Heinecke, W. S. Compel, D. L. Gustafson, C. J. Ackerson, et al. 2013. "Structure-Activity Relationships for biodistribution, Pharmacokinetics, and Excretion of Atomically Precise Nanoclusters in a Murine Model." *Nanoscale* 5 (21): 10525–10533.
- World Health Organization (WHO). 2009. *Principles for Modelling Dose-Response for the Risk Assessment of Chemicals*. International Programme on Chemical Safety. Geneva: WHO, 1–137. http://apps.who.int/iris/bitstream/10665/43940/1/9789241572392_eng.pdf.
- World Health Organization (WHO). 2010. *Characterization and Application of Physiologically Based Pharmacokinetic Models in Risk Assessment*. International Programme on Chemical Safety. Geneva: WHO, 1–91. http://www.who.int/ipcs/methods/harmonization/areas/pbpbk_models.pdf?ua=1.
- Xu, C., G. A. Tung, and S. Sun. 2008. "Size and Concentration Effect of Gold Nanoparticles on X-Ray Attenuation as Measured on Computed Tomography." *Chemistry of Materials* 20 (13): 4167–4169.
- Zhang X.-D., D. Wu, X. Shen, P.-X. Liu, N. Yang, B. Zhao, H. Zhang, et al. 2011. "Size-Dependent In Vivo Toxicity of PEG-Coated Gold Nanoparticles." *International Journal of Nanomedicine* 6: 2071–2081.